

AUTOMATIC VEHICLE TRAJECTORY DATA RECONSTRUCTION AT SCALE

Yanbing Wang, Corresponding Author

Vanderbilt University
yanbing.wang@vanderbilt.edu

Derek Gloudemans

Vanderbilt University
derek.gloudemans@vanderbilt.edu

Zi Nean Teoh

Vanderbilt University
zi.nean.teoh@vanderbilt.edu

Lisa Liu

Vanderbilt University
chuci.liu@vanderbilt.edu

Gergely Zachár

Vanderbilt University
gergely.zachar@vanderbilt.edu

William Barbour

Vanderbilt University
william.w.barbour@vanderbilt.edu

Daniel Work

Vanderbilt University
dan.work@vanderbilt.edu

ABSTRACT

Vehicle trajectory data has received increasing research attention over the past decades. With the technological sensing improvements such as high-resolution video cameras, in-vehicle radars and lidars, abundant individual and contextual traffic data is now available. However, though the data quantity is massive, it is by itself of limited utility for traffic research because of noise and systematic sensing errors, thus necessitates proper processing to ensure data quality. We draw particular attention to extracting high-resolution vehicle trajectory data from video cameras as traffic monitoring cameras are becoming increasingly ubiquitous. We explore methods for automatic trajectory data reconciliation, given “raw” vehicle detection and tracking information from automatic video processing algorithms. We propose a pipeline including **(a) an online data association algorithm to match** fragments that are associated to the same object (vehicle), which is formulated as a min-cost network flow problem of a graph, and **(b) a trajectory reconciliation method formulated as a quadratic program** to enhance raw detection data. The pipeline leverages vehicle dynamics and physical constraints to associate tracked objects when they become fragmented, remove measurement noise on trajectories and impute missing data due to fragmentations. The accuracy is benchmarked on a sample of manually-labeled data, which shows that the reconciled trajectories improve the accuracy on all the tested input data for a wide range of measures. An online version of the reconciliation pipeline is implemented and will be applied in a continuous video processing system running on a camera network covering a 4-mile stretch of Interstate-24 near Nashville, Tennessee.

Keywords: Trajectory data, data association, data reconciliation

INTRODUCTION

Motivation

Vehicle trajectory data is integral to the study of traffic dynamics. They reveal the relationship between individual traffic participants and the resulting traffic flow phenomena. The increasing volume of data sources is enabling revolutionary research on, for example, traffic flow theory (1–3) and traffic state estimation (4–6).

Not only a large scale is desired; the data must also have the microscopic fidelity (fine-grained vehicle positions) to validate and build realistic microscopic models. Accurate estimation of energy consumption also relies on vehicle-level detailed dynamics (7–9). High-quality trajectory data can close the gap for understanding microscopic traffic phenomena, such as lane-change and car-following (10–14) and the impact of mixed autonomy in traffic (15–17).

Moreover, being able to generate traffic measurements live is also important to facilitate traffic control. Real-time traffic control strategies such as variable speed limit and ramp metering (18), or Lagrangian control with connected and autonomous vehicles (19) require sufficiently prompt feedback and informative measurements to make decisions. To accomplish real-time deployment, we aim to build an efficient data reconciliation pipeline to handle streaming data with low latency.

Ultimately, vehicle and transportation technologies are trending towards "intelligent" and more autonomous solutions. Being able to measure the broader impact on traffic will be crucial in enabling future generations of traffic control and management. Now with advancement in camera resolutions and computer-vision algorithms for object detection and tracking, the process of getting reliable trajectory data can be greatly automated, yet issues on the quality of the data still remain. This work aims to provide a comprehensive pipeline to systematically rectify trajectory data produced by automatic computer vision algorithms. Leveraging physical constraints such as vehicle dynamics and state information, this pipeline outputs trajectories that significantly improve the validity and quality of the raw data. The work presented here is preliminary, but outlines the core methods needed for trajectory cleaning. Detailed algorithm tuning will increase the overall accuracy of the methods prior to deployment on a large scale system on a freeway testbed.

Challenges

One of the major challenges for this study is the lack of scope, quality, and resolution of highway traffic data, which is essential to understand the implication of deploying vehicle automation technology at scale.

Traditional traffic data collection mechanisms such as loop detectors provide low-frequency, aggregated features suitable for learning macroscopic characteristics; microscopic features, however, can be difficult to validate without the data at individual vehicle level. Vehicle on-board sensors and GPS measurements do not provide the necessary fidelity and/or completeness necessary for many applications such as vehicle energy/emission estimation (20, 21). Video-based trajectory data collection in conjunction with image processing algorithms can offer a "bird's eye" perspective and, with a dense deployment of cameras, can achieve complete spatial and temporal coverage of a roadway segment. Inaccuracies in such data – projection errors, occlusions, dimensions, and kinematic physicality (22), for example – need to be addressed. Automatic data reconciliation methods are needed to deal with massive volumes of trajectory data from traffic video processing.

A secondary challenge is that data reconciliation must be performed in real-time or with low latency, in order to enable the use of such data for intelligent traffic control. Therefore, fast

and online data reconciliation methods are to be explored.

Problem statement and contributions

Motivated by the lack of a high-quality, large-scale source of trajectory data necessary to assess the impact of driving behavior on large-scale traffic, the Tennessee Department of Transportation is building the I-24 MOTION testbed: an installation of nearly 300 high-resolution cameras across 4 miles of interstate highway. The continuous field of view provides for complete, high-resolution trajectories for nearly every individual vehicle on the roadway. A preliminary investigation on early versions of raw trajectories revealed various systematic errors caused by upstream computer vision detection and tracking (Figure 1). Data quality and reliability from video-based extraction is not well-validated and no methods exist for rectifying this trajectory data in a rigorous and time-efficient manner. Vehicle trajectory reconstruction aims at correcting the upstream detection and tracking errors without re-processing the videos, but instead leveraging physics-based knowledge, such as vehicle motions, from a transformed roadway coordinate system. We highlight the following contributions in this article:

- We propose an automatic trajectory data reconciliation pipeline for a modern traffic testbed. Specifically, the pipeline includes a) an online data association algorithm to solve a min-cost flow problem, which consequently matches fragments that belong to the same object, and b) a novel trajectory reconciliation algorithm, which is formulated as a quadratic program. It reconstructs realistic vehicle dynamics from disturbed detection data with systematic smoothing and outlier correction. The resulting trajectories automatically satisfy the internal consistency (differentiation of trajectories with speeds and accelerations).
- We provide evaluations on the trajectory quality including dynamics analysis, error statistics and runtime analysis. Results show that the reconciled trajectories improve a variety of measures on various configurations of upstream video processing algorithms.

This work, although still in progress, illustrates the first step towards automatic and online trajectory data reconciliation from video-based data extraction. Future work will focus on fine tuning the parameters associated with the proposed algorithms to further enhance the data quality.

RELATED WORK

Vehicle trajectory datasets

Trajectories from a common reference system serve as the ultimate empirical data to study traffic dynamics. Throughout the literature, we have found a growing volume of trajectory datasets collected at various scales through different sensing mechanisms. We summarize these in Table 1.

Small-scale trajectory data is usually collected via vehicles that have been equipped with high-accuracy GPS sensors (23–26) and other in-vehicle sensors. Unlike conventional probe vehicles or floating cars, vehicles currently collect their position data with significantly higher spatial and temporal resolution levels to obtain high-quality trajectory data (27). Data collected from a combination of in-vehicle sensors such as radars, LiDAR and cameras provides ambient information, which can be useful for traffic flow studies as well as for training and testing AI algorithms for autonomous driving. Readers are directed to references such as (28, 29) for a comprehensive discussion on such dataset.

Image sensors and video processing algorithms associated with overhead cameras or Unmanned Aerial Systems (UAV) have become increasingly powerful as a large-scale trajectory data

TABLE 1 Video-based trajectory data comparison. VMT: vehicle miles traveled

Dataset	Year	Context	Camera config	Road segment	VMT	Hours of recording
NGSIM	2006	Highway	8 cameras	600m	18,000	0.75
pNeuma	2018	Urban arterial	10 drones	10km	N/A	59
highD	2018	Highway	1 drone	420m	28,000	147
Automatum	2021	Highway	Overhead drones	N/A	18,724	30
HIGH-SIM	2021	Highway	Aerial cameras	2,438m	N/A	2
I-24 MOTION	2022	Highway	300 4K cameras	4 miles	200M/yr (expected)	continuous stream

source. The seminal work is the Next Generation Simulation (NGSIM) dataset (30) developed in early 2000s, which is a collection of real-world trajectories, based on the use of cameras mounted on tall buildings and covering approximately 600-meter long roadway sections with a frequency of 10 Hz in several US locations. More recently in the highD dataset (31), videos were recorded by overhead flying drones (4096 × 2160 pixels, 25 fps), which provided much higher-quality videos than that of the NGSIM dataset (21). HighD provides highway trajectories covering 420m of road segment, for a total of 28,000 vehicle miles traveled. pNEUMA large-scale field experiment (32) aimed to record traffic streams in a multi-modal congested environment over an urban area using UAV. The dataset was generated by a swarm of 10 drones hovering over a traffic intensive area of 1.3 km² in the city center of Athens, Greece, covering more than 100 km-lanes of road network at 25 Hz. Most recently, Automatum dataset became available (33), which covers 12 characteristic highway-like scenes from 30 hours of drone videos. HIGH-SIM (34) is another high-quality highway trajectory dataset extracted from aerial video data. The videos were collected by three 8K cameras in a helicopter over an 8000 ft long segment of the I-75 freeway in Florida for 2 hours. The dataset covers a wide range of traffic characteristics. A comparison across selected datasets can be viewed from Table 1. Other examples and discussion on their usage in traffic studies can be found in a comprehensive survey, such as (20).

Data extraction and quality assessment

Raw trajectories from video footage are usually obtained from a *tracking-by-detection* framework (35, 36), where a set of object detections for all frames are linked across time to form continuous trajectories. The detected bounding boxes are then transformed to a common reference system (e.g., global positioning system) for meaningful interpretation of dynamics. One of the errors we aim to reconcile is tracking discontinuity due to, for example, noisy detection, inevitable object occlusion and switching camera field of views, which results in track fragmentations. The first problem to address is data association, with is given a set of detections, identify their origin (objects that they are associated with). Data association problems can be difficult when the tracking produces large fragmentations or when the detections have false alarms or missing detections, which are common in real-world video-based detection systems.

Different approaches for data association have been proposed depending on the association

criteria, complexity of object motion and the computation requirements. In general, these approaches differ from their choices of 1) matching cost (sometimes termed as probability, affinity, energy or confidence) and 2) matching criteria (global minimization of a cost, greedy approach, hierarchical matching etc.), which result in various problem formulations. The matching cost reflects kinematic (position and velocity) and attribute information (shape affinity), and the matching criteria directly drives the algorithm to solve the data association problem.

Graph-based formulations provide efficient algorithms for finding the global min-cost tracking solutions. The tracks (or detections) can be naturally represented as the nodes of a graph and the pair-wise matching costs can be represented as graph edges. The general data association problem is finding the least-cost set cover on the track graph (37). Studies such as (38–40) have explored efficient algorithms related to bipartite matching and min-cost flow. Interested readers are referred to a recent survey, such as (41) on this topic.

Although trajectory data serves as the fundamental building block for traffic studies, many works (21, 22, 42) raised the issue of the quality of the seminal NGSIM data, including nonphysical kinematics and inter-vehicle distance. The importance for data postprocessing is also emphasized in (13, 14, 20, 22). Montanino and Punzo (43) undertook one of the most thorough efforts of data reconciliation by applying a series of smoothing operations on the dataset. They posed the smoothing and reconstruction as a nonlinear, non-convex optimization problem, as to find the minimum local smoothing window subject to kinematic constraints. Other data postprocessing efforts (42, 44, 45) also performed data reconciliation considering realistic vehicle kinematics and driving dynamics. Although comprehensive, these works provide ad-hoc treatments for specific sources of errors and rely on multiple iterations of smoothing, which cannot be applied for the streaming setting. In this work we demonstrate a more efficient alternative for trajectory reconciliation that applies to streaming data.

PROBLEM FORMULATION

We focus on addressing two types of issues stemming from the raw tracking data. The first is a *fragmentation*, in which an object (vehicle) is tracked as two or more objects at different times, generally because it transitions through one camera field of view to another or is occluded by a larger vehicle for a sustained period. It results in discontinuity in tracking and broken trajectories. The second type of error is a *detection inaccuracy* which is caused by either a missing detection, an error in vehicle position estimation, or a non-rectilinear shapes produced by the object detector (shown in Figure 1). Given these known errors, we propose a two-step trajectory reconstruction approach: 1. a *min-cost flow* formulation for fragments association, and 2. a *quadratic programming* for trajectory data rectification (detection inaccuracy correction) based on dynamics.

The methods proposed below are performed on the 2D raw trajectories in real-world coordinates, assuming a fixed point on each vehicle travels in 2D planar motion. It follows a normal-tangential coordinate system, i.e., the x -axis is parallel to the lane lines, including on a curve. We also let positive x correspond to east-bound traffic and negative correspond to west-bound, to distinguish directions. The y -axis is perpendicular to x .

In this section, we outline the problem formulation for multi-object tracking as a minimum-cost flow (MCF) of a graph. Solving for MCF on a track graph results in trajectory sets that have the highest *maximum a posteriori* (MAP) probability. The problem formulation is explained in literature such as (39, 46), and therefore only highlighted briefly in this section.

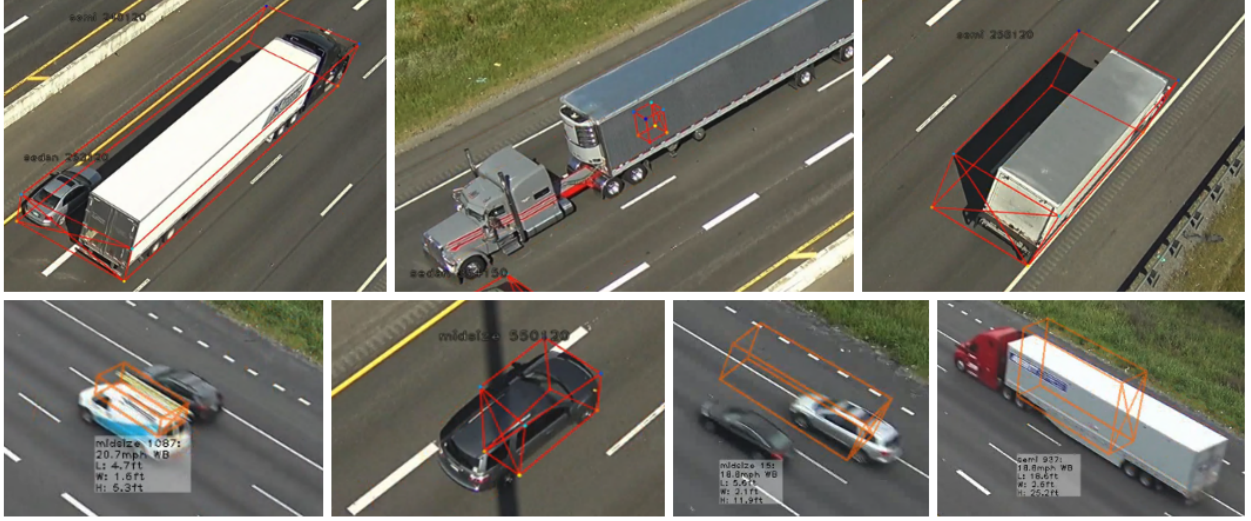


FIGURE 1 Examples of common inaccuracies from upstream video processing algorithms: missing detection, inaccurate localization, and non-rectilinear shape.

Preliminary: MCF and successive shortest path

A fragment with index k is denoted as $\phi_k = \{p_1, \dots, p_n\}$, which consists of a series of positional data ordered by time (frame). Each data point p_i is a vector containing timestamp, x and y position of a fixed point on the bounding box. We are given a set of fragments as input $\Phi = \{\phi_i\}$. A trajectory $\tau_k = \{\phi_{k_1}, \dots, \phi_{k_n}\}$ consists of one or multiple fragments. A set of such trajectories form a trajectory set hypothesis $T = \{\tau_1, \dots, \tau_K\}$. Assuming that fragments are conditionally independent and identically distributed random variables (i.i.d.), the fragment association step aims at finding T^* , the hypothesis with the highest MAP:

$$\begin{aligned}
 T^* &= \operatorname{argmin}_T P(T|\Phi) \\
 &= \operatorname{argmin}_T P(\Phi|T)P(T) \\
 &= \operatorname{argmin}_T \prod_i P(\phi_i|T) \prod_{\tau_k \in T} P(\tau_k)
 \end{aligned} \tag{1}$$

$$\text{s.t. } \tau_k \cap \tau_l = \emptyset, \forall k \neq l,$$

with a non-overlapping trajectory constraint, since each fragment can belong to at most one trajectory. The likelihood $P(\phi_i|T) = P(\phi_i) = \beta_i$ indicates the probability that fragment i is a false positive and thus should not be included in the trajectory hypothesis. The prior of a trajectory can be modeled as a Markov chain:

$$P(\tau_k) = P_{\text{enter}}(\phi_{k_1}) \prod_{i=1}^{n-1} P(\phi_{k_{i+1}}|\phi_{k_i}) P_{\text{exit}}(\phi_{k_n}), \tag{2}$$

where $P_{\text{enter}}(\phi_{k_1})$ and $P_{\text{exit}}(\phi_{k_n})$ denote the probabilities that ϕ_{k_1} starts the trajectory and ϕ_{k_n} ends the trajectory, respectively. Taking the negative logarithm of (1), the MAP problem becomes equiv-

alent to the following integer program:

$$\underset{f_i, f_{i,j}, f_i^{en}, f_i^{ex}}{\text{minimize}} \sum_i c_i f_i + \sum_i c_i^{en} f_i^{en} + \sum_{i,j} c_{i,j} f_{i,j} + \sum_i c_i^{ex} f_i^{ex} \quad (3a)$$

$$\text{s.t. } f_i, f_{i,j}, f_i^{en}, f_i^{ex} \in \{0, 1\}, \quad (3b)$$

$$f_i^{en} + \sum_j f_{j,i} = f_i = f_i^{ex} + \sum_j f_{i,j}, \forall i \in V \setminus \{s, t\}, \quad (3c)$$

where

$$c_i^{en} = -\log P_{enter}(\phi_i), c_i^{ex} = -\log P_{exit}(\phi_i), c_{i,j} = -\log P(\phi_i | \phi_j), c_i = -\log \frac{1 - \beta_i}{\beta_i}. \quad (4)$$

The decision variables are binary according to constraint(3b). f_i indicates whether ϕ_i should be included in any trajectory, f_i^{en} and f_i^{ex} determine whether a trajectory starts or ends with ϕ_i , respectively. $f_{i,j}$ indicates if fragment ϕ_j is an immediate successor of ϕ_i . Constraint (3c) ensures non-overlapping trajectories.

In seminal work (39), it is shown that (3) has a natural graph interpretation, and solving for (3) is equivalent to solving the min-cost-flow of a tracklet graph, which has a polynomial solution (47). The graph is constructed such that each fragment ϕ_i is represented as two nodes u_i and v_i , with a directed edge (u_i, v_i) and a cost indicating *inclusion* of ϕ_i ; edges between two fragments ϕ_i and ϕ_j are represented as (v_i, u_j) , with the cost related to the likelihood of ϕ_j following ϕ_i . The edge direction implies the sequential order between fragments. The resulting graph is therefore a directed acyclic graph (DAG), see Figure 2. Furthermore, the graph has a source node s that has an incident edge to every u , and a sink node t that every v points to. We denote the weighted DAG as $G(V, E, C)$, with node set V , edge set E and edge weights (costs) C . The data association problem can be formulated as finding a set of non-overlapping $s - t$ paths on a DAG with lowest total cost, or finding “flows” from s to t that result in the minimum total cost.

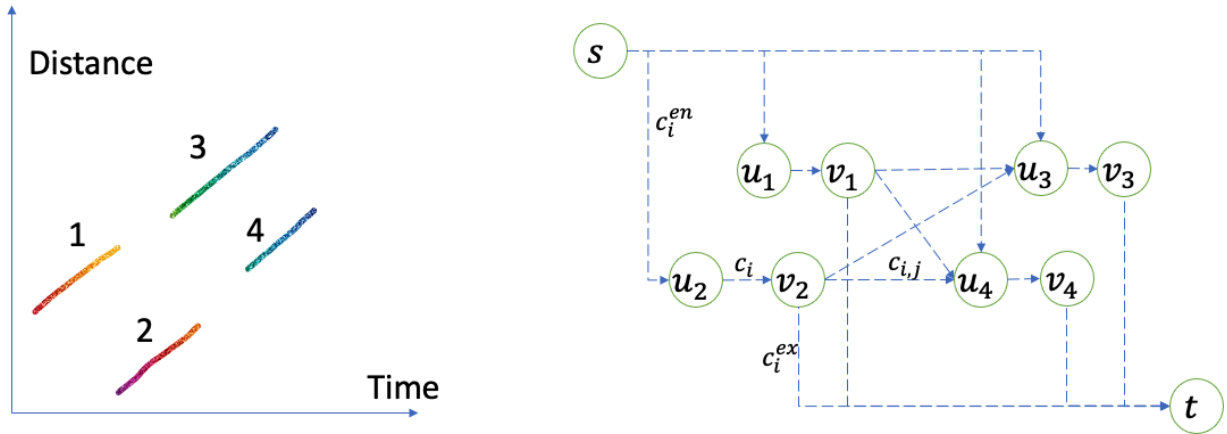


FIGURE 2 Left: fragments in time-space coordinates; right: fragments as a directed acyclic graph (DAG). All edges have a unit capacity and varying costs, labeled as $c_i, c_{i,j}, c_i^{en}$ and c_i^{ex} .

One efficient algorithm is the *successive shortest path* (SSP) (48) based on Ford-Fulkerson’s method for incremental improvement. The idea is to iteratively look for and push a feasible flow in the residual network that has a negative cost. The algorithm terminates when no more negative cycles can be found (optimality condition). Many tracking approaches have improved upon the

generic SSP algorithm (e.g., (46, 49)). We direct interested readers the above reference for the details and proof of correctness of this algorithm, and only provide an outline in Algorithm 1.

Min-cost-flow for fragment association

First, a tracking graph $G(V, E, C)$ is constructed from Φ (ConstructTrackletGraph), and we iteratively look for the shortest path from s to t (ShortestPath). If the path cost is negative, then update the residual graph according to Definition 1 (PushFlow). When the iteration stops (no more negative-cost $s - t$ path can be found), the assignment, or the trajectories, can be extracted by traversing along the residual edges from t to s (FlowToTrajectories).

The residual graph G_r is an important notion to understand the min-cost-flow algorithm, and is defined below:

Definition 1. The residual graph $G_r(V, E_r, C_r)$ for the tracking graph $G(V, E, C)$ with respect to a flow f is generated by replacing each edge $(u, v) \in E$ by two residual edges $(u, v) \in E_r$, where $(u, v) \in E_r$ has cost $C_r(u, v) = C(u, v)$ and residual capacity $r_{uv} = 1 - f_{uv}$, while $(v, u) \in E_r$ has cost $C_r(v, u) = -C(u, v)$ and residual capacity $r_{vu} = f_{uv}$.

Algorithm 1 Successive shortest path for min-cost-flow on a tracklet graph

Input: Set of fragments $\Phi = \{\phi_i\}$

Result: Set of trajectories $T = \{\tau_k\}$

$G(V, E, C) \leftarrow \text{ConstructTrackletGraph}(\Phi)$

$f \leftarrow 0$

$G_r^{(0)} \leftarrow G$

$\pi^{(0)}, d^{(0)} \leftarrow \text{ShortestPath}(G_r^{(0)})$ //run single source shortest path from s . π is the shortest path from s to t , d is a distance (cost) map from s to any other nodes in G

$k = 0$

while $d^{(k)}(t) < 0$ **do**

 //Update residual graph

$G_r^{(k+1)} \leftarrow \text{PushFlow}(G_r^{(k)}, \pi^{(k)})$

 //Find the next shortest path from s to t

$\pi^{(k+1)}, d^{(k+1)} \leftarrow \text{ShortestPath}(G_r^{(k+1)})$

$k \leftarrow k + 1$

end

$T \leftarrow \text{FlowToTrajectories}(G_r^{(k)})$

The worst-case run time for 1 is $\mathcal{O}(K(n \log(n) + m))$, where n is the number of nodes in graph, m is the number of edges and K is the total number of flow (trajectories). It is shown in a later work (50) that a better performance can be achieved for solving minimum-cost circulation of a modified tracking graph.

Online MCF

The streaming data coming from I-24 MOTION testbed necessitates an online and memory-bounded version of Algorithm 1. In other words, the tracking graph G is dynamic: new fragments are added and older fragments are removed from the graph constantly. A naive online extension of Algorithm 1 is to run the same algorithm on each updated graph. However, it is inefficient because the

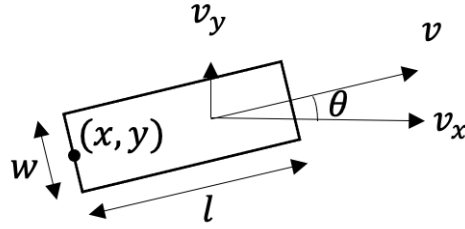


FIGURE 3 A simple 2D vehicle model

majority of the graph remains the same and the majority of the computation on the shortest path is wasted. This opens opportunities for algorithm engineering improvements to improve performance.

A possible improved online MCF can be achieved by modifying the tracking graph 2 into an equivalent one as shown in (50). Instead of connecting all the post nodes v'_s to t , they will be directed back to s , and the original MCF problem is equivalent to finding the min-cost circulation on the modified graph G . The algorithm proceeds by adding fragments ϕ'_s ordered by last timestamp to the so called residual graph G_r^- one at a time, to obtain a new graph G_r^- . For each iteration, we search for the least-cost negative cycle Γ in the graph and push flow through the cycle to obtain the updated residual graph G_r^+ . It can be proved that pushing flow through Γ , G_r^+ , contains the min-cost circulation because the flow is feasible and no further negative cycles can be found in G_r^+ .

Trajectory reconciliation

After applying fragment association, the next step is to rectify the stitched, raw trajectories with denoising, imputation and smoothing operations. Instead of ad-hoc correcting each source of the detection errors shown in Figure 1, we treat all noises and errors in a one-step approach to rectify them all at once. To simplify the problem, we consider a 2D vehicle motion model, with independent longitudinal (x) and lateral (y) dynamics. This allows us to decompose the problem to solving two independent 1D reconciliation problems. The reconciled trajectories automatically satisfy the state consistency amongst the orders of differentiation, i.e., the finite-difference of position is speed and the finite-difference of speed is acceleration, etc.

We use the following notations. Each trajectory τ_i includes the following features (features are the same for all trajectories, therefore the index i is dropped for simplicity): let $\mathbf{x} = [x[1], x[2], \dots, x[N]]^T$ be the back-center x -position vector for N timesteps, and similarly let \mathbf{y} be the time-series of the back-center y -position; $\mathbf{v}_x = [v_x[1], v_x[2], \dots, v_x[N-1]]^T$ is the time-series of speed in the longitudinal direction (x -axis), and similarly \mathbf{v}_y is the time-series of speed in the lateral component (y -axis). The acceleration \mathbf{a} and jerk \mathbf{j} use the same 2D representation. Lastly, l, w represent the vehicle length and width, respectively. The vehicle dynamics model can be seen in Figure 3

Consider the following discrete-time 3rd order 1D motion model in either longitudinal or lateral direction (the same method is applied for x -component and y -component dynamics. We

demonstrate on x -component only):

$$x[t+1] = x[t] + v[t]\Delta T$$

$$v[t+1] = v[t] + a[t]\Delta T \quad (5)$$

$$a[t+1] = a[t] + j[t]\Delta T,$$

with ΔT as the timestep. Notice that the finite-difference method decrements the dimension of time-series as an increase of derivative order, i.e., $\mathbf{x} \in \mathbb{R}^N$, $\mathbf{v} \in \mathbb{R}^{N-1}$, $\mathbf{a} \in \mathbb{R}^{N-2}$ and $\mathbf{j} \in \mathbb{R}^{N-3}$. Eq (5) can be written in matrix multiplication form:

$$\mathbf{v} = D^{(1)}\mathbf{x}$$

$$\mathbf{a} = D^{(2)}\mathbf{x} \quad (6)$$

$$\mathbf{j} = D^{(3)}\mathbf{x},$$

$D^{(k)} \in \mathbb{R}^{(N-k) \times N}$ represents the k^{th} -order differentiation operator, specifically

$$D^{(1)} = \frac{1}{\Delta T} \begin{bmatrix} -1 & 1 & 0 & \dots & 0 & 0 & 0 \\ 0 & -1 & 1 & \dots & 0 & 0 & 0 \\ \vdots & \vdots & \vdots & & \vdots & \vdots & \vdots \\ 0 & 0 & 0 & \dots & -1 & 1 & 0 \\ 0 & 0 & 0 & \dots & 0 & -1 & 1 \end{bmatrix}$$

$$D^{(2)} = \frac{1}{\Delta T^2} \begin{bmatrix} 1 & -2 & 1 & 0 & \dots & 0 & 0 & 0 \\ 0 & 1 & -2 & 1 & \dots & 0 & 0 & 0 \\ \vdots & \vdots & \vdots & \vdots & & \vdots & \vdots & \vdots \\ 0 & 0 & 0 & 0 & \dots & 1 & -2 & 1 \end{bmatrix}$$

$$D^{(3)} = \frac{1}{\Delta T^3} \begin{bmatrix} -1 & 3 & -3 & 1 & \dots & 0 & 0 & 0 & 0 \\ \vdots & \vdots & \vdots & \vdots & & \vdots & \vdots & \vdots & \vdots \\ 0 & 0 & 0 & 0 & \dots & -1 & 3 & 3 & 1 \end{bmatrix}$$

Consider corrupted measurement \mathbf{z} which contains missing data (indicated by the observation operator H), noises \mathbf{w} and outliers \mathbf{e} :

$$\mathbf{z} = H\mathbf{x} + \mathbf{w} + \mathbf{e}, \quad \mathbf{z} \in \mathbb{R}^M, \mathbf{w} \in \mathbb{R}^M, \mathbf{e} \in \mathbb{R}^M, H \in \mathbb{R}^{M \times N}, \quad (7)$$

and missing data exists if $M < N$. We aim to find the reconstructed position $\hat{\mathbf{x}}$ that is smooth in k^{th} -order derivatives. The idea is to use a combination of Ridge and Lasso regression (51), to simultaneously handle noises and outliers, assuming outliers are sparse and noises have small magnitude:

$$(\hat{\mathbf{x}}, \hat{\mathbf{e}}) = \underset{\mathbf{x}, \mathbf{e}}{\operatorname{argmin}} \|\mathbf{z} - H\mathbf{x} - \mathbf{e}\|_2^2 + \lambda_2 \|D^{(k)}\mathbf{x}\|_2^2 + \lambda_1 \|\mathbf{e}\|_1. \quad (8)$$

The first term of the cost function in (8) penalizes the data-fitting error on the non-missing entries. The second term regularize the smoothness of the position vector, by penalizing the l_2 -norm of a higher derivative (e.g., jerk). The third term regularizes the sparsity of the outliers. Note that (8) can be written into a quadratic programming form by converting the l_1 penalization to a linear programming with linear inequality constraints (52) (53). The problem can be solved with a convex programming solver such as *cvxopt* (54). Note that above formulation rectifies the trajectory of each vehicle independently of another. After treatment (8), further investigation is needed to determine if, for example, considering vehicular interactions in the optimization formulation (e.g., with additional non-collision constraint) is required.

The 2D dynamics can be obtained by solving two independent optimization problems of

TABLE 2 Ground Truth Dataset Statistics

Fields	Ground Truth (GT) values
Length of video recording (sec)	113
Length of road segment (ft)	2073
Total number of vehicle annotations	176,243
No. lanes	8
No. trajectories	321
Trajectory lengths median (ft)	2073.9
Speed (ft/sec) (mean, stdev, max)	(114.0, 49.1, 471.7)

form (8) for both longitudinal and lateral dynamics.

The lateral movement follows the same discrete-time dynamics as (5). Let the solution for solving (8) for the longitudinal movement be $(\hat{\mathbf{x}}, \hat{\mathbf{e}}_x)$, and the solution for the lateral movement be $(\hat{\mathbf{y}}, \hat{\mathbf{e}}_y)$. The rectified steering angle $\hat{\theta} = [\theta[1], \dots, \theta[N-1]]^T$ can be calculated in the end as

$$\hat{\theta} = \tan^{-1} \left(\frac{D^{(1)}\hat{\mathbf{y}}}{D^{(1)}\hat{\mathbf{x}}} \right). \quad (9)$$

EXPERIMENTS

The proposed 2-step data reconciliation pipeline is applied on four different upstream vehicle detection and tracking algorithms on the same recorded videos. These algorithms are sufficiently varied to provide a wide range of input data (termed as RAW 1-4), with qualities measured in detection precision (0.55 to 0.75), recall (0.54 to 0.66), fragmentations (1.23 to 4.56 per ground truth vehicle) and trajectory derivative quantities (acceleration and velocity distributions) – these numerical measures are based on standard MOTA metrics outlined in (55), and are later summarized in Table 3-6. The corresponding reconciled results after running the 2-step postprocessing pipeline are termed as REC 1-4. We note the experiments are a first step towards refining the algorithms, for example identifying optimal parameters, cost models etc. Here we provide initial evidence that the methods are capable of reducing errors over a range of datasets, rather than optimizing parameters to remove all errors on a given dataset.

Datasets description

All evaluations are performed on an internal dataset obtained from the I-24 MOTION validation system, to be subsequently released to the public. The dataset consists of approximately 175,000 vehicle annotations spanning 90 seconds of video capturing free-flow traffic from each of 18 traffic cameras, with ground truth vehicle positions annotated manually for all vehicles within the video sequences. Table 2 summarizes this dataset in more detail.

Evaluation metrics

Vehicles tracking and trajectory reconciliation performance can be evaluated with standard *multi-object-tracking* (MOT) metrics, specified in (55–58). The following metrics for evaluation are used:

- *Precision*: number of detected objects over sum of detected and false positives.
- *Recall*: number of detections over number of objects.

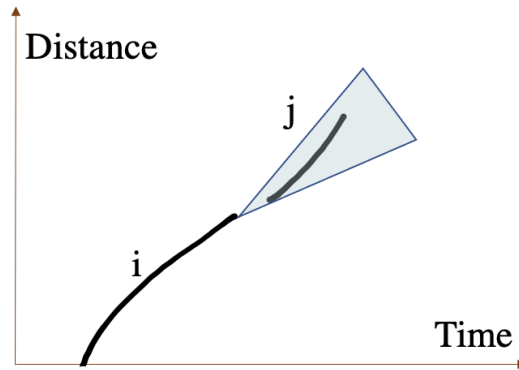


FIGURE 4 Probability of fragment ϕ_i after the last measurement of ϕ_i is represented as a cone. The matching cost of ϕ_i and ϕ_j is determined by the negative log likelihood of ϕ_j given the cone probability.

- *Switches per GT*: total number of track switches per ground truth trajectory.
- *Fragments per GT*: total number of switches from tracked to not tracked per ground truth trajectory.
- *Multi-object-tracking accuracy (MOTA)*: an aggregated measure from 0-1 to indicate tracking performance. It is detection errors (false negatives and false positives) and fragmentations normalized by the total number of true detections.
- *Multi-object-tracking precision (MOTP)*: the total error in estimated position for matched prediction and ground truth pairs over all time, averaged by the total number of matches made.

Other statistics are computed to qualitatively assess the trajectories:

- Trajectory lengths distribution
- Speed distribution (calculated using finite-difference)
- Acceleration distribution (calculated using finite-difference)
- *Mean absolute errors (MAE)* on position: the average absolute error of predicted position and the ground truth position for the matched instances.

Implementation details

In this section, we describe the computation of edge costs for min-cost flow and the choice of parameters λ_1 and λ_2 for solving the trajectory rectification problem 8.

The probabilities of a trajectory starts or ends with a fragment P_{enter} and P_{exit} is determined by the ratio of the true number of trajectories and the predicted number of trajectories. The fragment linking costs $P(\phi_i|\phi_j)$ can be modeled by (a combination of) dynamics, shape affinity and the time interval between the two fragments. We implemented a version that considers the dynamics only, as it is shown to properly represent the matching probabilities.

The general idea is, if ϕ_j is indeed a continuation of ϕ_i but the object tracking is broken due to, e.g., object occlusion, then the projected position of ϕ_i at the time of ϕ_j has a high chance of overlapping with the actual detection of ϕ_j . The probability of track i at the time of ϕ_j follows a stochastic process, with the mean \hat{p}_i being the projected position of track i given ϕ_i , and the

variance increases with respect to Δt , the time elapsed since the end of ϕ_i , t_e^i , i.e.,

$$p_i(t_e^i + \Delta t) = \hat{p}_i(t_e^i + \Delta t) + \eta_i(\Delta t), \text{ and } \eta_i(\Delta t) \sim \mathcal{N}(0, \alpha \Delta t). \quad (10)$$

The uncertainty $\eta_i(\Delta t)$ follows a Wiener random process, with zero-mean and variance $\alpha \Delta t$ growing linearly with Δt (see Figure 4). The projected mean of position is:

$$\hat{p}_i(t) = v_i t + \bar{p}_i, \quad (11)$$

where $v_i = [v_{x,i}, v_{y,i}]^T$ and $\bar{p}_i = [x_i, y_i]^T$ can be determined using, for example, linear regression.

Finally, the matching cost is the negative log likelihood of ϕ_j given the probabilities computed from ϕ_i :

$$\Lambda(\phi_i, \phi_j) = \frac{1}{2N_j} \sum_{t_j \in [t_s^j, t_e^j]} \log(\alpha(t_j - t_e^i)) + \frac{1}{2N_j} \sum_{t_j \in [t_s^j, t_e^j]} \frac{(p_j(t_j) - \hat{p}_i(t_j))^2}{\alpha(t_j - t_e^i)}, \quad (12)$$

where N_j is the number of measurements of ϕ_j . t_s^j and t_e^j are the start and end timestamp of ϕ_j , and $p_j(t_j)$ is the measurement of ϕ_j at t_j .

After fragment association, the next step is to impute missing data, correct for outliers and smooth the trajectories all in one step, by solving an optimization problem (8). A grid search is conducted to find the best parameters λ_1 and λ_2 that balance each term in the cost function (8). We pre-tune the parameters to be $\lambda_1 = 1.2e-3$ and $\lambda_2 = 1.67e-2$ based on empirical assessment of a subset of trajectories. The parameter tuning is challenging due to the fact that vehicle dynamics are subject to quantization errors that still exist in the ground truth, as the ground truth bounding boxes are human-annotated on independent video frames. We demonstrate the capacity the above choice of parameters to bring close the speed and acceleration to a more realistic range, but note that a detailed parameter optimization that generalizes to a range of datasets is part of our ongoing effort to operationalize the described methods.

Results

Evaluation results are obtained by benchmarking RAW 1-4 and the corresponding REC 1-4 against the same manually-labeled ground truth data, and are summarized in Table 3-6. Results show that given varying levels of raw tracking (RAW 1-4) as inputs, the 2-step reconciliation outputs (REC 1-4) always improve a wide range of metrics.

Data reconciliation improves precision and recall for about 15-25% as compared to the raw tracking data. The improvement is achieved by correctly associating fragments together and imputing the missing detections between the fragments, which results in an increase of true positives and decrease of false negatives. Furthermore, outliers are rejected in the trajectory rectification step (8), reducing the false positives as well. Consequently, the aggregated score MOTA improves. MOTP and position MAE improve mainly due to outlier removal and smoothing effect of the trajectory rectification step.

In addition, a few statistics on the dynamical information of the trajectories are computed. The speed is computed using finite difference of the distance traveled (trajectory lengths), and similarly the acceleration is computed by finite difference of the speed. Figures 5-8 show that in general, RECs produce longer trajectories due to the fragment association step (fragments per GT is reduced up to 90%). Another noticeable improvement is on the acceleration distribution: the regularization terms in (8) of data reconciliation attribute to narrower (or more consistent) distribution. It is expected, however, that a fixed choice of parameter λ_1 and λ_2 may not be generalizable to all trajectories. It is possible that additional tuning is necessary to generate data of a more feasible dynamics. Here we illustrate that the data reconciliation approach is leading to promising

TABLE 3 Evaluation results for the first input dataset.

Metrics / Statistics	Raw Tracking 1 (RAW 1)	Reconciled 1 (REC 1)
Precision \uparrow	0.67	0.78 (+16.4%)
Recall \uparrow	0.55	0.66 (+20.0%)
MOTA \uparrow	0.50	0.57 (+14.0%)
MOTP \uparrow	0.57	0.65 (+14.0%)
Fragments per GT \downarrow	4.56	0.47 (-90.0%)
Switches per GT \downarrow	0.76	0.30 (-60.5%)
Position MAE (ft) \downarrow	4.25	2.95 (-30.5%)
No. unique trajectories	655	478
Trajectory lengths (ft) (mean, stdev, max)	(857.9, 677.0, 2054.6)	(1161.6, 697.3, 2054.6)
Speed (ft/sec) (mean, stdev, max)	(115.2, 44.5, 596.7)	(107.3, 19.7, 297.8)
Acceleration (ft/sec ²) (mean, stdev, max)	(246.0, 1449.7, 6887.6)	(4.1, 53.7, 772.5)

TABLE 4 Evaluation results for the second input dataset

Metrics / Statistics	RAW 2	REC 2
Precision \uparrow	0.55	0.63 (+14.5%)
Recall \uparrow	0.66	0.80 (+18.2%)
MOTA \uparrow	0.39	0.49 (+25.6%)
MOTP \uparrow	0.56	0.63 (+12.5%)
Fragments per GT \downarrow	1.23	0.25 (-79.7%)
Switches per GT \downarrow	0.34	0.05 (-85.3%)
Position MAE (ft) \downarrow	4.13	2.87 (-30.5%)
No. unique trajectories	483	373
Trajectory lengths (ft) (mean, stdev, max)	(1224.3, 554.0, 2128.0)	(1489.9, 479.8, 2128.0)
Speed (ft/sec) (mean, stdev, max)	(108.8, 16.1, 191.6)	(106.6, 11.4, 167.9)
Acceleration (ft/sec ²) (mean, stdev, max)	(-3.78, 25.6, 101.8)	(-0.12, 2.3, 17.7)

direction.

Lastly, we conduct a brief run-time analysis of the reconciliation step. To speed up solving (8) for long trajectories, a rolling horizon reconciliation approach is applied. For benchmarking, we choose a 3-sec (90 timestamps) rolling time window, and only apply the reconciled results from the first 50 timestamps. This allows the total run time to be approximately linear with respect to the length of the trajectory. For light traffic (flow is about 30 vehicles/lane/min), it amounts to approximately 400 trajectories per min for 4 miles and 8 lanes, per the testbed configuration. The reconciliation step takes around 17 seconds to process 1 min of traffic, meeting the real-time processing requirement. Likewise, in heavy traffic (120 vehicles/lane/min) one minute of data is processed in 50 seconds, still meeting the real-time requirement.

CONCLUSION AND FUTURE WORK

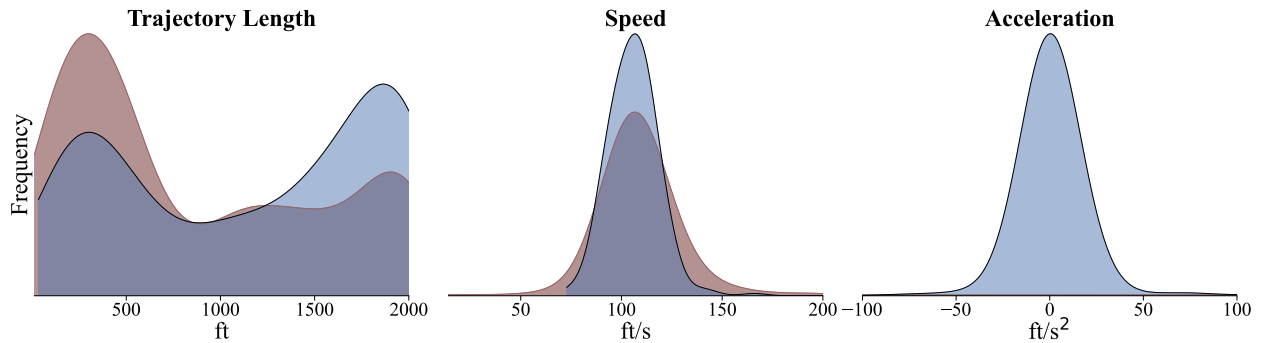
High-quality trajectory data can close the gap for understanding microscopic traffic phenomena. A real-world live testbed like I-24 MOTION helps researchers to understand the impact of mixed

TABLE 5 Evaluation results for the third dataset

Metrics / Statistics	RAW 3	REC 3
Precision \uparrow	0.75	0.88 (+17.3%)
Recall \uparrow	0.57	0.68 (+19.3%)
MOTA \uparrow	0.55	0.63 (+14.5%)
MOTP \uparrow	0.56	0.64 (+14.3%)
Fragments per GT \downarrow	1.88	0.23 (-87.8%)
Switches per GT \downarrow	0.56	0.09 (-83.9%)
Position MAE (ft) \downarrow	4.53	3.12 (-31.1%)
No. unique trajectories	610	420
Trajectory lengths (ft) (mean, stdev, max)	(892.3, 593.9, 1995.0)	(1319.6, 511.3, 1995.0)
Speed (ft/sec) (mean, stdev, max)	(106.9, 11.1, 145.9)	(106.1, 10.3, 141.1)
Acceleration (ft/sec ²) (mean, stdev, max)	(-2.47, 61.8, 358.5)	(-0.26, 2.21, 23.1)

TABLE 6 Evaluation results for the fourth dataset

Metrics / Statistics	RAW 4	REC 4
Precision \uparrow	0.70	0.83 (+18.5%)
Recall \uparrow	0.54	0.67 (+24.7%)
MOTA \uparrow	0.59	0.67 (+13.6%)
MOTP \uparrow	0.56	0.65 (+16.1%)
Fragments per GT \downarrow	4.44	0.51 (-88.5%)
Switches per GT \downarrow	1.31	0.39 (-70.2%)
Position MAE \downarrow	4.65	3.33 (-28.4%)
No. unique trajectories	992	572
Trajectory lengths (ft) (mean, stdev, max)	(568.0, 560.7, 1955.0)	(1014.1, 644.3, 1998.7)
Speed (ft/sec) (mean, stdev, max)	(110.0, 20.8, 279.0)	(105.5, 10.8, 142.6)
Acceleration (ft/sec ²) (mean, stdev, max)	(-62.2, 1847.7, 9433.5)	(1.46, 23.4, 255.4)

**FIGURE 5** Distributions of trajectory lengths (left), average speed (middle) and acceleration (right) for RAW 1 (red) and REC 1 (blue).

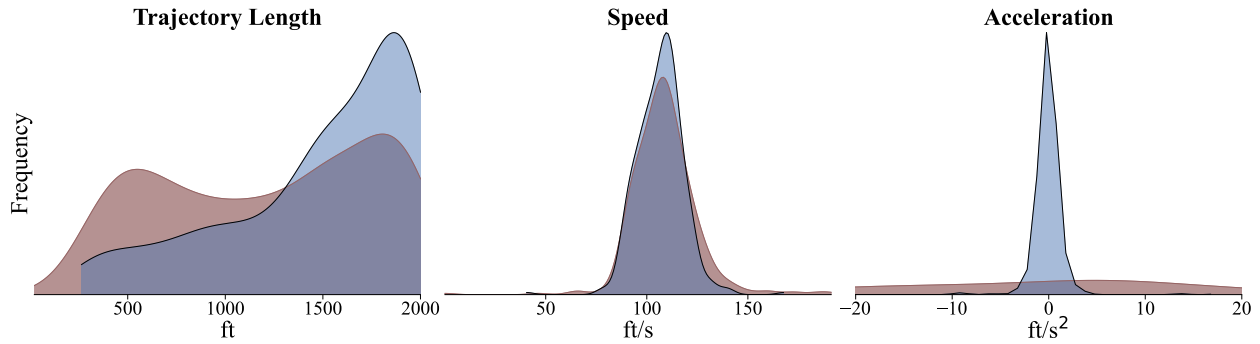


FIGURE 6 Distributions of trajectory lengths (left), average speed (middle) and acceleration(right) for RAW 2 (red) and REC 2 (blue).

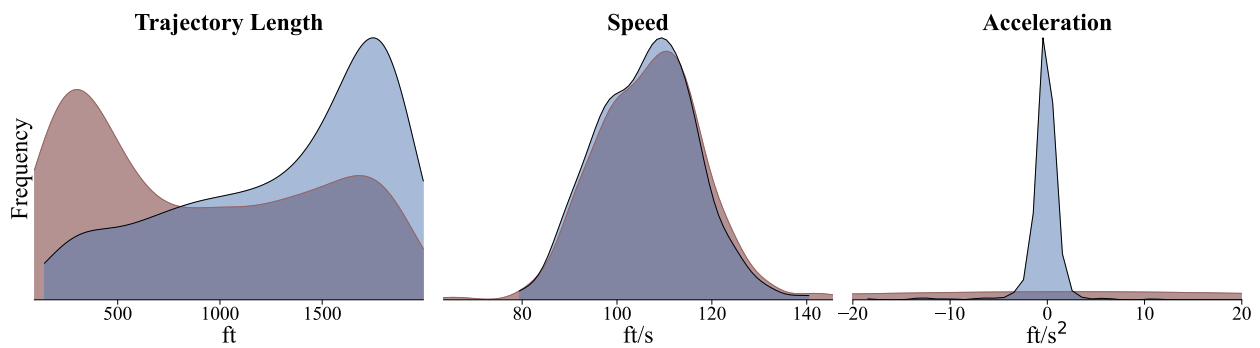


FIGURE 7 Distributions of trajectory lengths (left), average speed (middle) and acceleration(right) for RAW 3 (red) and REC 3 (blue).

autonomy in traffic. However, data produced by cameras and upstream computer vision algorithms still lacks high quality to be ready for research use. In this paper we demonstrate a two-step data postprocessing pipeline to automatically reconcile detection and tracking data. The pipeline includes a fragment association algorithm to solve an online min-cost flow problem, and a trajectory rectification approach formulated as a quadratic programming. The accuracy and run-time analysis are benchmarked on a manually-labeled ground truth data. Results show that the two-step treatments improve a variety of trajectory quality measures, given different configurations of upstream video processing algorithms. Noticeably, it significantly improves the velocity and acceleration dynamics, despite the parameter tuning for the trajectory smoothing step is only preliminary. This proposed pipeline has high promises to replace previous manual efforts on data cleaning.

For future work, a few algorithmic improvements can be made on existing methods to potentially address issues in real data. For example, a multi-vehicle reconciliation formulation can be considered to account for potential collisions. Furthermore, different edges costs and an exhaustive parameter tuning need to be performed to improve the current results.

ACKNOWLEDGEMENT

This study is based upon work supported by the National Science Foundation (NSF) under Grant No. 1837652, the NSF Graduate Research Fellowship Grant No. DGE-1937963 and the USDOT Dwight D. Eisenhower Fellowship program under Grant No. 693JJ32245006.

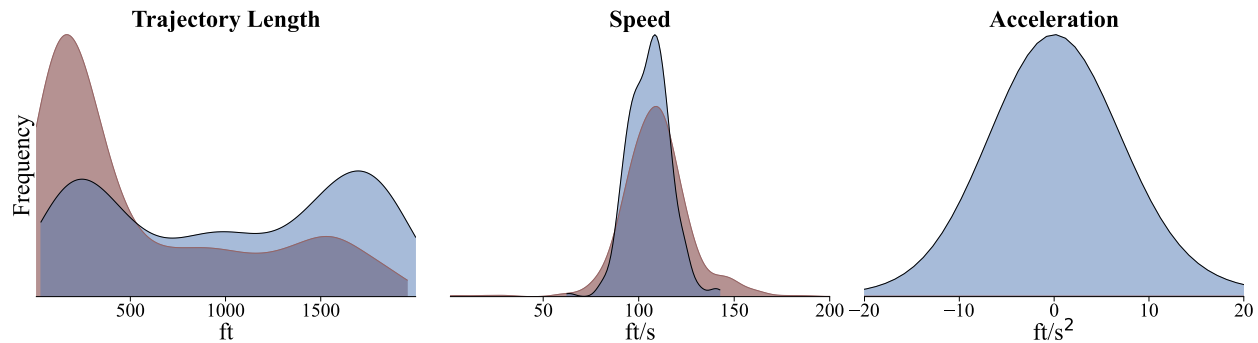


FIGURE 8 Distributions of trajectory lengths (left), average speed (middle) and acceleration(right) for RAW 4 (red) and REC 4 (blue).

REFERENCES

1. Treiterer, J. and J. Myers, The hysteresis phenomenon in traffic flow. *Transportation and traffic theory*, Vol. 6, 1974, pp. 13–38.
2. Hoogendoorn, S. and V. Knoop, Traffic flow theory and modelling. *The transport system and transport policy: an introduction*, 2013, pp. 125–159.
3. Greenberg, H., An analysis of traffic flow. *Operations research*, Vol. 7, No. 1, 1959, pp. 79–85.
4. Seo, T., A. M. Bayen, T. Kusakabe, and Y. Asakura, Traffic state estimation on highway: A comprehensive survey. *Annual reviews in control*, Vol. 43, 2017, pp. 128–151.
5. Wang, Y. and M. Papageorgiou, Real-time freeway traffic state estimation based on extended Kalman filter: a general approach. *Transportation Research Part B: Methodological*, Vol. 39, No. 2, 2005, pp. 141–167.
6. Tao, S., V. Manolopoulos, S. Rodriguez Duenas, and A. Rusu, Real-time urban traffic state estimation with A-GPS mobile phones as probes. *Journal of Transportation Technologies*, Vol. 2, No. 1, 2012, pp. 22–31.
7. Fiori, C., K. Ahn, and H. A. Rakha, Power-based electric vehicle energy consumption model: Model development and validation. *Applied Energy*, Vol. 168, 2016, pp. 257–268.
8. Fiori, C., V. Marzano, V. Punzo, and M. Montanino, Energy consumption modeling in presence of uncertainty. *IEEE Transactions on Intelligent Transportation Systems*, Vol. 22, No. 10, 2020, pp. 6330–6341.
9. Oh, G., D. J. Leblanc, and H. Peng, Vehicle energy dataset (VED), a large-scale dataset for vehicle energy consumption research. *IEEE Transactions on Intelligent Transportation Systems*, 2020.
10. Gazis, D. C., R. Herman, and R. B. Potts, Car-following theory of steady-state traffic flow. *Operations Research*, Vol. 7, No. 4, 1959, pp. 499–505.
11. Gipps, P. G., A behavioural car-following model for computer simulation. *Transportation Research Part B: Methodological*, Vol. 15, No. 2, 1981, pp. 105–111.
12. Schakel, W. J., V. L. Knoop, and B. van Arem, Integrated lane change model with relaxation and synchronization. *Transportation Research Record*, Vol. 2316, No. 1, 2012, pp. 47–57.
13. Kesting, A. and M. Treiber, Calibrating car-following models by using trajectory data:

- Methodological study. *Transportation Research Record*, Vol. 2088, No. 1, 2008, pp. 148–156.
14. Treiber, M. and A. Kesting, Traffic flow dynamics. *Traffic Flow Dynamics: Data, Models and Simulation*, Springer-Verlag Berlin Heidelberg, 2013.
 15. Stern, R. E., S. Cui, M. L. Delle Monache, R. Bhadani, M. Bunting, M. Churchill, N. Hamilton, H. Pohlmann, F. Wu, B. Piccoli, et al., Dissipation of stop-and-go waves via control of autonomous vehicles: Field experiments. *Transportation Research Part C: Emerging Technologies*, Vol. 89, 2018, pp. 205–221.
 16. Gunter, G., D. Gloudemans, R. E. Stern, S. McQuade, R. Bhadani, M. Bunting, M. L. Delle Monache, R. Lysecky, B. Seibold, J. Sprinkle, B. Piccoli, and D. B. Work, Are commercially implemented adaptive cruise control systems string stable? *arXiv:1905.02108*, 2019.
 17. Yang, D., A. Kuijpers, G. Dane, and T. van der Sande, Impacts of large-scale truck platooning on Dutch highways. *Transportation research procedia*, Vol. 37, 2019, pp. 425–432.
 18. Carlson, R. C., I. Papamichail, M. Papageorgiou, and A. Messmer, Optimal motorway traffic flow control involving variable speed limits and ramp metering. *Transportation science*, Vol. 44, No. 2, 2010, pp. 238–253.
 19. Vinitzky, E., K. Parvate, A. Kreidieh, C. Wu, and A. Bayen, Lagrangian Control through Deep-RL: Applications to Bottleneck Decongestion. In *2018 21st International Conference on Intelligent Transportation Systems (ITSC)*, 2018, pp. 759–765.
 20. Li, L., R. Jiang, Z. He, X. M. Chen, and X. Zhou, Trajectory data-based traffic flow studies: A revisit. *Transportation Research Part C: Emerging Technologies*, Vol. 114, 2020, pp. 225–240.
 21. Coifman, B. and L. Li, A critical evaluation of the Next Generation Simulation (NGSIM) vehicle trajectory dataset. *Transportation Research Part B: Methodological*, Vol. 105, 2017, pp. 362–377.
 22. Punzo, V., M. T. Borzacchiello, and B. Ciuffo, On the assessment of vehicle trajectory data accuracy and application to the Next Generation SIMulation (NGSIM) program data. *Transportation Research Part C: Emerging Technologies*, Vol. 19, No. 6, 2011, pp. 1243–1262.
 23. Jiang, R., M.-B. Hu, H. M. Zhang, Z.-Y. Gao, B. Jia, Q.-S. Wu, B. Wang, and M. Yang, Traffic experiment reveals the nature of car-following. *PloS one*, Vol. 9, No. 4, 2014, p. e94351.
 24. Jiang, R., M.-B. Hu, H. Zhang, Z.-Y. Gao, B. Jia, and Q.-S. Wu, On some experimental features of car-following behavior and how to model them. *Transportation Research Part B: Methodological*, Vol. 80, 2015, pp. 338–354.
 25. Coifman, B., M. Wu, K. Redmill, and D. A. Thornton, Collecting ambient vehicle trajectories from an instrumented probe vehicle: High quality data for microscopic traffic flow studies. *Transportation Research Part C: Emerging Technologies*, Vol. 72, 2016, pp. 254–271.
 26. Huang, Y.-X., R. Jiang, H. Zhang, M.-B. Hu, J.-F. Tian, B. Jia, and Z.-Y. Gao, Experimental study and modeling of car-following behavior under high speed situation. *Transportation research part C: emerging technologies*, Vol. 97, 2018, pp. 194–215.

27. Guo, Q., L. Li, and X. J. Ban, Urban traffic signal control with connected and automated vehicles: A survey. *Transportation research part C: emerging technologies*, Vol. 101, 2019, pp. 313–334.
28. Makridis, M., K. Mattas, A. Anesiadou, and B. Ciuffo, *openACC. An open database of car-following experiments to study the properties of commercial ACC systems*, 2020.
29. Kang, Y., H. Yin, and C. Berger, Test Your Self-Driving Algorithm: An Overview of Publicly Available Driving Datasets and Virtual Testing Environments. *IEEE Transactions on Intelligent Vehicles*, Vol. 4, No. 2, 2019, pp. 171–185.
30. NGSIM, *The Next Generation Simulation Program*. <http://ops.fhwa.dot.gov/trafficanalysistools/ngsim.htm>, 2006, u.S. Department of Transportation Federal Highway Administration.
31. Krajewski, R., J. Bock, L. Kloecker, and L. Eckstein, The highd dataset: A drone dataset of naturalistic vehicle trajectories on german highways for validation of highly automated driving systems. In *2018 21st International Conference on Intelligent Transportation Systems (ITSC)*, IEEE, 2018, pp. 2118–2125.
32. Barmponakis, E. and N. Geroliminis, On the new era of urban traffic monitoring with massive drone data: The pNEUMA large-scale field experiment. *Transportation research part C: emerging technologies*, Vol. 111, 2020, pp. 50–71.
33. Spannaus, P., P. Zechel, and K. Lenz, AUTOMATUM DATA: Drone-based highway dataset for the development and validation of automated driving software for research and commercial applications. In *2021 IEEE Intelligent Vehicles Symposium (IV)*, IEEE, 2021, pp. 1372–1377.
34. Shi, X., D. Zhao, H. Yao, X. Li, D. K. Hale, and A. Ghiasi, Video-based trajectory extraction with deep learning for High-Granularity Highway Simulation (HIGH-SIM). *Communications in Transportation Research*, Vol. 1, 2021, p. 100014.
35. Kalal, Z., K. Mikolajczyk, and J. Matas, Tracking-Learning-Detection. *IEEE Transactions on Pattern Analysis and Machine Intelligence*, Vol. 34, No. 7, 2012, pp. 1409–1422.
36. Andriluka, M., S. Roth, and B. Schiele, People-tracking-by-detection and people-detection-by-tracking. In *2008 IEEE Conference on Computer Vision and Pattern Recognition*, 2008, pp. 1–8.
37. Chong, C.-Y., Graph approaches for data association. In *2012 15th international conference on information fusion*, IEEE, 2012, pp. 1578–1585.
38. Castnnón, G. and L. Finn, Multi-target tracklet stitching through network flows. In *2011 Aerospace Conference*, IEEE, 2011, pp. 1–7.
39. Zhang, L., Y. Li, and R. Nevatia, Global data association for multi-object tracking using network flows. In *2008 IEEE Conference on Computer Vision and Pattern Recognition*, IEEE, 2008, pp. 1–8.
40. Vyahhi, N., S. Bakiras, P. Kalnis, and G. Ghinita, Tracking moving objects in anonymized trajectories. In *International Conference on Database and Expert Systems Applications*, Springer, 2008, pp. 158–171.
41. Rakai, L., H. Song, S. Sun, W. Zhang, and Y. Yang, Data association in multiple object tracking: A survey of recent techniques. *Expert Systems with Applications*, Vol. 192, 2022, p. 116300.

42. Thiemann, C., M. Treiber, and A. Kesting, Estimating acceleration and lane-changing dynamics from next generation simulation trajectory data. *Transportation Research Record*, Vol. 2088, No. 1, 2008, pp. 90–101.
43. Montanino, M. and V. Punzo, Trajectory data reconstruction and simulation-based validation against macroscopic traffic patterns. *Transportation Research Part B: Methodological*, Vol. 80, 2015, pp. 82–106.
44. Hamdar, S. H. and H. S. Mahmassani, *Driver car-following behavior: From discrete event process to continuous set of episodes*. Transportation Research Board 87th Annual Meeting, 2008.
45. Duret, A., C. Buisson, and N. Chiabaut, Estimating individual speed-spacing relationship and assessing ability of Newell’s car-following model to reproduce trajectories. *Transportation research record*, Vol. 2088, No. 1, 2008, pp. 188–197.
46. Wang, C., Y. Wang, Y. Wang, C.-T. Wu, and G. Yu, muSSP: Efficient min-cost flow algorithm for multi-object tracking. *Advances in Neural Information Processing Systems*, Vol. 32, 2019.
47. Ford, L. R. and D. R. Fulkerson, Maximal flow through a network. *Canadian journal of Mathematics*, Vol. 8, 1956, pp. 399–404.
48. Ahuja, R. K., T. L. Magnanti, and J. B. Orlin, *Network flows*. Cambridge, Mass.: Alfred P. Sloan School of Management, Massachusetts . . . , 1988.
49. Lenz, P., A. Geiger, and R. Urtasun, Followme: Efficient online min-cost flow tracking with bounded memory and computation. In *Proceedings of the IEEE International Conference on Computer Vision*, 2015, pp. 4364–4372.
50. Wang, C., Y. Wang, and G. Yu, Efficient Global Multi-object Tracking Under Minimum-cost Circulation Framework. *IEEE transactions on pattern analysis and machine intelligence*, 2020.
51. Zou, H. and T. Hastie, Regularization and variable selection via the elastic net. *Journal of the royal statistical society: series B (statistical methodology)*, Vol. 67, No. 2, 2005, pp. 301–320.
52. Chen, S. S., D. L. Donoho, and M. A. Saunders, Atomic decomposition by basis pursuit. *SIAM review*, Vol. 43, No. 1, 2001, pp. 129–159.
53. Boyd, S., S. P. Boyd, and L. Vandenberghe, *Convex optimization*. Cambridge university press, 2004.
54. Vandenberghe, L., The CVXOPT linear and quadratic cone program solvers. *Online: <http://cvxopt.org/documentation/coneprog.pdf>*, 2010.
55. Bernardin, K. and R. Stiefelhagen, Evaluating multiple object tracking performance: the clear mot metrics. *EURASIP Journal on Image and Video Processing*, Vol. 2008, 2008, pp. 1–10.
56. Milan, A., L. Leal-Taixé, I. Reid, S. Roth, and K. Schindler, MOT16: A benchmark for multi-object tracking. *arXiv preprint arXiv:1603.00831*, 2016.
57. Li, Y., C. Huang, and R. Nevatia, Learning to associate: Hybridboosted multi-target tracker for crowded scene. In *2009 IEEE conference on computer vision and pattern recognition*, IEEE, 2009, pp. 2953–2960.
58. Ristani, E., F. Solera, R. Zou, R. Cucchiara, and C. Tomasi, Performance measures and a data set for multi-target, multi-camera tracking. In *European conference on computer vision*, Springer, 2016, pp. 17–35.